Global and Planetary Change 123 (2014) 13–26

Contents lists available at ScienceDirect

Global and Planetary Change

journal homepage: www.elsevier.com/locate/gloplacha

Extreme cyclone wave climate in the Southwest Pacific Ocean: Influence of the El Niño Southern Oscillation and projected climate change

Scott A. Stephens *, D.L. Ramsay

National Institute of Water and Atmospheric Research, PO Box 11115, Hamilton 3251, New Zealand

ARTICLE INFO

Article history:
Received 24 June 2014
Received in revised form 2 October 2014
Accepted 9 October 2014
Available online 14 October 2014

Keywords:
tropical cyclones
El Niño Southern Oscillation
climate change
extreme wave
Pacific Ocean

ABSTRACT

This paper describes the first use of a stochastic cyclone model (SCM) to quantify the extreme significant wave height from tropical cyclones across the Southwest Pacific Ocean. The median extreme significant wave heights across the entire SW Pacific Ocean were 7.5, 10 and 11 m for annual exceedance probabilities (AEPs) of 0.1, 0.02 and 0.01 respectively. Maximum significant wave heights in the region were approximately 1.5 times these values for the same AEP. Tables of extreme significant wave heights are provided for selected inhabited locations. The SCM was used to quantify the effects of the El Niño-Southern Oscillation (ENSO) on extreme significant wave heights, and also the effects of projected climate change on cyclone intensity and frequency of occurrence. West of the International Dateline in the region of the Vanuatu archipelago, the extreme cyclone wave climate was relatively consistent during all phases of the ENSO cycle, but highest during El Niño. Cyclone formation and propagation eastward of the Dateline are more likely to occur during El Niño conditions, however these cyclones tended to be more intense, particularly during extreme El Niño events, leading to a higher long-term extreme wave climate in the eastern SW Pacific, despite the relatively low cyclone observation rate there. Simulations of climate change cyclone intensity increases of 10–20% of the most intense cyclones (categories 4 and 5) along with 10–20% reduction in number of cyclones indicated little change in extreme significant wave heights for low-occurrence AEPs of 1/20 or less. These changes were much less than induced by present-day ENSO variability, suggesting that future changes in extreme wave climate will be sensitive to climate change influences on the frequency and intensity of ENSO events. These results are significant in the light of indications that the frequency of extreme El Nino events might double in response to greenhouse warming.

1. Introduction

Tropical cyclones (TCs) are among the world's most destructive natural disasters, bringing strong winds, heavy rainfall, large waves and storm surges that devastate property and cause loss of life (e.g. Chu and Wang, 1998; Sinclair, 2002; Terry and Gienko, 2010; Diamond et al., 2012). Predictions of TC frequency and magnitude enable disaster managers to design appropriate preparations in advance of the event that can significantly reduce risk, including loss of life. The ecosystems and economies of small island nation states and territories of the tropical SW Pacific region are widely agreed to be among the most vulnerable to climate variability and weather extremes anywhere in the world (Diamond et al., 2012). Many low-lying atolls in the SW Pacific Ocean are vulnerable to large cyclone waves that pump water onto narrow fringing reefs and can raise water levels by meters. Yet growing human populations and tourism are placing increasing development pressure on small atolls that often have limited development space in what are commonly narrow and vulnerable coastal land areas.

There is a need to define the frequency–magnitude relationship, otherwise known as the extreme value distribution, for cyclone wave hazard exposure to help decision makers in many fields such as wastewater management, road works, electricity, health, coastal zone management, civil defense and insurance. The objective of an extreme value analysis is to quantify the stochastic behavior of a process at unusually large values and the usual process is to fit an appropriate extreme value model to the most extreme values within an instrumental or observation-based measurement record (Coles, 2001). The problem is that long-duration measurements for cyclone-induced waves (and/or storm surges) don't exist in the SW Pacific Ocean (e.g. James and Mason, 2005; McInnes et al., 2014). Wave hindcast models are available (e.g. Gorman et al., 2003a, b), but under-predict the most extreme wave heights due mainly to under-representation of the most intense wind speeds in the wind reanalyses used to drive the wave hindcast models (e.g. Stephens and Gorman, 2006). Wave records from satellite altimetry provide a robust means of quantifying the spatial distribution of the mean wave climate (e.g. Challenor et al., 1990; Tournadre and Ezraty, 1990; Young, 1994, 1999), and estimates of the extreme wave climate have been made

* Corresponding author. Tel.: +64 7 856 1745.
E-mail addresses: Scott.Stephens@niwa.co.nz (S.A. Stephens), Doug.Ramsay@niwa.co.nz (D.L. Ramsay).

http://dx.doi.org/10.1016/j.gloplacha.2014.10.002

using altimetry (e.g. Alves and Young, 2003; Vinoth and Young, 2011). However, wave altimeters pass over the same point only once about every 10 days, requiring spatial averaging assuming homogeneous wave conditions over a broad area (e.g. 0.5 × 0.5°–4 × 4°) to obtain sufficient temporal density. Because the median radius for maximum wind of tropical cyclones in the SW Pacific is about 0.5° (from IBTrACS data Knapp et al. (2010)), and the peak wave production occurs in a relatively small leading quadrant of the cyclone (e.g. Young, 1988), satellite altimetry also under-samples (and underestimates) the extreme cyclone wave record.

In this study, we describe a new stochastic cyclone model (SCM) to predict frequency–magnitude relationships for significant wave height, peak wave period and inverse-barometer storm surge, and apply it to determine the extreme cyclone significant wave climate for the SW Pacific Ocean, for the first time. We examine the influence of ENSO climate variability on the extreme wave climate and compare and contrast present-day climate variability effects with those from projected climate change.

2. Background

2.1. Stochastic cyclone models

Lack of direct cyclone wind and wave records has led to the development of mathematical SCM, which are based on statistical re-sampling of tropical cyclone data records. Much of the TC data worldwide consists of the best estimates of storm position and intensity at 6-hourly intervals, which are termed best-track data (Knapp et al., 2010). SCM have become an accepted approach for estimating wind speeds and wave conditions for the design of structures and assessment of cyclone risk. Russell (1971) applied the first SCM to predict cyclone wind speed, with numerous examples since (e.g. Georgiou et al., 1983; Bretschneider, 1990; Vickery et al., 2000b; James and Mason, 2005; Emanuel et al., 2006; Hall and Jewson, 2007; Rumpf et al., 2007, 2010; Yasuda et al., 2010; McInnes et al., 2014). To provide frequency–magnitude relationships necessary for hazard exposure quantification, a typical SCM approach is to fit statistical distributions to the best-track observations to produce a cyclone climatology. Monte Carlo techniques are then often used to randomly sample the statistical climatology, to represent 1000s of years of cyclone events, which are then coupled to dynamic or parametric wave models to simulate cyclone impacts. Using Monte Carlo simulations, sufficient cyclone impacts are simulated to calculate the frequency–magnitude relationship at a site of interest.

In the northern hemisphere, SCMs have been used to simulate the spatial distribution of tropical cyclones (e.g. Hall and Jewson, 2008; Emanuel and Jagger, 2010; Rumpf et al., 2010; Yonekura and Hall, 2011; Jagger and Elsner, 2012), and also the key cyclone parameters such as cyclone central pressure that are required to drive numerical models for the prediction of cyclone wind, wave and storm-surge (e.g. Chu and Wang, 1998; Casson and Coles, 2000; Kossin and Camargo, 2009). Like this study, there are several studies that have further used SCMs to undertake site-specific extreme-value analyses of tropical cyclone hazard (e.g. Russell, 1971; Georgiou et al., 1983; Vickery and Twisdale, 1995; Chouinard et al., 1997; Vickery et al., 2000a, b; Wang and Chan, 2002; Madsen and Jakobsen, 2004; James and Mason, 2005; Emanuel et al., 2006; Rumpf et al., 2007, 2009; Yasuda et al., 2010; McInnes et al., 2014). There are few published studies where cyclone hazards have been statistically quantified in the SW Pacific. James and Mason (2005) developed a SCM for the Coral Sea and applied it to simulate frequency–magnitude relationships for cyclone central pressure impacting the north-east coast of Australia. McInnes et al. (2014) combined a SCM with a hydrodynamic surge model to compute storm surge climatology for Fiji, and Daniel et al. (2009) applied a hydrodynamic model to simulate storm surge for selected historical cyclone events impacting New Caledonia and French Polynesia.

2.2. ENSO, climate change and TC relationships

The El Nino Southern Oscillation (ENSO) is well known to influence the frequency and spatial distribution of cyclones in the world's oceans, and has a strong influence on the pattern of cyclone occurrence and resulting cyclone hazard in the SW Pacific (Revell and Goulter, 1986; Grant and Walsh, 2001; Sinclair, 2002; Chand and Walsh, 2009, 2010; Kuleshov et al., 2010; Terry and Gienko, 2010; Ramsay et al., 2012; Diamond et al., 2013). TC generation in the SW Pacific is strongly modulated by the South Pacific Convergence Zone (SPCZ), which is a major source of rainfall and an incubation region for tropical cyclones (Vincent, 1994; Salinger et al., 1995; Folland et al., 2002; Vincent et al., 2011; Diamond et al., 2013). El Niño conditions are accompanied by a northward and eastward movement of the SPCZ. ENSO modulates sea-surface temperature (SST) that constrains the location of the SPCZ, which in turn strongly modulates atmospheric circulation patterns and constrains tropical cyclogenesis to occur preferentially within 10° south of the SPCZ (Vincent et al., 2011). During El Niño events the eastern boundary of the Western Pacific warm pool (the region covered by water warmer than ~28 °C) and the atmospheric convective zone move eastwards to just east of the International Dateline (Santoso et al., 2013; Cai et al., 2014), allowing TC formation further east than normal. Thus, ENSO variability strongly influences patterns of TC generation and intensity. Furthermore, the 1982/83 and 1997/98 seasons were classified as extreme El Niño events (Vincent et al., 2011; Cai et al., 2014), during which a pronounced eastward extension of the west Pacific warm pool and development of atmospheric convection resulted in extreme swings of the SPCZ to a zonal orientation (Vincent et al., 2011), and an unprecendented number of intense TCs further north and east than usual in the vicinity of French Polynesia (e.g. Revell and Goulter, 1986). The cyclone observational database on which the SCM is based includes multiple ENSO cycles that include the two extreme El Niño events, thus it makes sense to use the SCM to investigate ENSO influence on cyclone extreme wave hazard by sampling the best-track cyclone database conditionally according to an ENSO index.

Climate change is expected to affect frequency and intensity of tropical cyclones. As yet there are no statistically significant trends in the number or intensity of tropical cyclones in the South Pacific Ocean (Kuleshov et al., 2010). Global climate model simulations suggest that the intensity of the strongest tropical cyclones is likely to increase globally, but some simulations suggest increases in the intensities of the strongest storms in the SW Pacific, while others suggest no change, or decrease (Knutson et al., 2010; Walsh et al., 2012). The review by Walsh et al. (2012) indicates changes in maximum wind speed in the South Pacific ranging from −22% to +1%. Walsh et al. (2004) indicated a +26% increase in the number of TCs with central pressure < 970 mb, and Leslie et al. (2007) showed a doubling of TCs with wind speeds > 30 m s^{-1} by 2050s. The overwhelming majority of global climate model simulations suggest fewer tropical cyclones in the South Pacific region in a warmer world: projections range from large decreases, with numbers falling by more than half, to one simulation giving a slight increase in numbers (Walsh et al., 2012). Likewise, late twenty-first-century model projections indicate decreases ranging from −6 to −34% globally, with a comparatively more robust decrease for the Southern Hemisphere mean counts (Knutson et al., 2010). The application of a SCM allows us to explore the effects of climate change on extreme wave climate by perturbing the intensity and occurrence rate of cyclones to represent the effects of climate change, relative to recent historical observations.

Cai et al. (2014) presented climate modeling evidence for a doubling in the occurrences of extreme El Niño in the future in response to greenhouse warming, which has ramifications for cyclone wind, wave and storm surge hazard throughout the SW Pacific. Sea-levels are rising and will continue to do so for many centuries (Church et al., 2006; IPCC, 2007; Hannah and Bell, 2012), resulting in increasing baseline elevations for wave attack at the coast and compounding any future increase in the extreme cyclone wave climate.

Our knowledge of the frequency–magnitude relationship for TC hazard is based on observations made under recent climatic conditions, but the degree to which climate change will influence TC hazard is an important question that can aid decision making for the future. By using the SCM to examine the effects of present-day ENSO variability on the frequency and magnitude of extreme cyclone waves, we can infer the effects of climate change in terms of both potential mean changes and changes in ENSO variability. Since cyclone waves are generated by wind energy transfer to the sea surface, the cyclone wave height trends also reflect cyclone wind speed and storm surge trends.

3. Methodology

The SCM works as follows: (1) obtain, quality-control and subsample cyclone best-track data; (2) fit empirical models to the best-track data to create a cyclone climatology; (3) simulate cyclone climatology at target locations by drawing thousands of Monte Carlo samples from the empirical cyclone climatology; (4) simulate the spatial distribution of atmospheric pressure, wind and waves from the simulated cyclone climatology, using parametric cyclone models; and (5) calculate frequency–magnitude relationships for wave height and period, and inverse-barometer storm-surge at the target locations. In this manuscript we focus on results for significant wave height only.

The SCM simulates cyclone properties based on sampling the empirical distributions of historical cyclone observations. It uses five observed cyclone parameters: (1) central mean sea level pressure; (2) maximum 10-minute sustained wind speed; (3) radius to maximum wind (RMW); (4) propagation speed; and (5) propagation direction.

TC best-track data have been routinely observed by satellite since 1969/1970, providing a more comprehensive and consistent coverage than pre-satellite observations (Knapp et al., 2010). We obtained the International Best Track Archive for Climate Stewardship (IBTrACS) best-track position and intensity dataset for the South Pacific ocean (Knapp et al., 2010), which contains datasets from numerous meteorological stations worldwide. The data period included observations from November 1969 to April 2009. We used data from: (1) World Meteorological Organization (which provides a single intensity report per observation time selected by the official WMO agency using only WMO-sanctioned forecast agencies); (2) U.S. Department of Defense Joint Typhoon Warning Center (JWTC); (3) Australian Bureau of Meteorology; (4) Fiji Meteorological Service; (5) Meteorological Service of New Zealand; and (6) C. Neumann's Southern Hemisphere data (e.g. Neumann et al., 1997). A single cyclone is often represented in multiple datasets. The JWTC dataset contained the most RMW data and so was prioritized where radius to maximum wind data were present. Otherwise the dataset with the most complete intensity record was used for each cyclone, or, finally, was prioritized in the order listed above. Observations from the post-1969/70 satellite era were used and only cyclones that attained a minimum central pressure of 995 hPa or lower were considered. The model was constrained to the SW Pacific Ocean using satellite observations east of 140°E longitude and north of −45°S latitude (Fig. 1).

To account for ENSO variability in the model the cyclone observational dataset was separated into Neutral, El Niño and La Niña phases of the ENSO cycle (Fig. 1) using the NINO 3.4 sea-surface-temperature anomaly index (Rayner et al., 2003). The NINO 3.4 region is bounded by 120°W–170°W and 5°S–5°N. An El Niño or La Niña event was identified if the 5-month running-average of the NINO 3.4 index exceeded +0.4 °C for El Niño or −0.4 °C for La Niña, for at least 6 consecutive months, following Trenberth (1997). The use of a 6-month window (as opposed to a shorter window) helps to reduce signal noise and draw out the strongest and most persistent El Niño and La Niña events from the index (Fig. 2). According to this definition, Neutral, La Niña and El Niño conditions occurred 42, 31 and 27% of the time respectively, for the 1969/70–2008/09 observation period.

Maps of average annual number of TCs (Fig. 3) show substantial shifts in the positions of maximum TC occurrences as well as changes in the intensity of occurrence maxima, with more cyclones close to the Australian coast and New Zealand during La Niña conditions than during El Niño conditions. There is a higher probability of cyclone activity east of the International Dateline during El Niño. These findings mirror those of Kuleshov et al. (2008), even though they counted cyclones over a different period (1949/50–2005/06) and used a different ENSO index to define ENSO phases. The rate of TC occurrence was higher during Neutral conditions than either El Niño or La Niña (Fig. 3), with 46% 25% and 29% of TCs occurring during Neutral, La Niña and El Niño conditions respectively.

Diamond et al. (2013) used a coupled ENSO index (CEI) based on both the NINO 3.4 sea-surface-temperature index and the southern oscillation atmospheric-pressure index to separate ENSO into nine unique CEI phases of which 7 were observed, enabling a clearer separation of ENSO-related cyclone tracks compared to the NINO 3.4 index alone. However, separation of the cyclone database into 7 smaller CEI subsets would have reduced the sampling base of the SCM for each ENSO phase, increasing statistical uncertainty in the model predictions. For our purposes, the NINO 3.4 index classification provides sufficient detail to demonstrate important ENSO-related features of extreme cyclone wave distribution.

3.1. Model algorithm

The model executes the following sequential steps: (1) A target location at which cyclone hazard information is required is first defined. (2) A 'local' model is then defined by a target window encompassing the target location that ensures simulations are based on historical observations within a 3° radius, the choice of which is explained later. This follows the basic assumption of all SCMs that cyclones located in similar areas of the ocean behave similarly. The aim is to now simulate cyclones in this target window so that the simulated population has the same statistical properties as the historical observations from within the target window (see items 5–7 below and later sections on defining cyclone parameters for more detail). Thousands or years' worth of cyclones is then simulated, enabling robust frequency–magnitude calculations, while preserving the statistical properties of the original observational dataset. (3) Empirical cyclone observation rates are calculated based on the historical rate of 6-hourly observations within the target window. These are calculated separately for Neutral, El Niño and La Niña ENSO conditions. (4) The required number of Monte Carlo simulations is calculated based on historical observation rates, and required minimum annual exceedance probability statistics and associated confidence intervals. An index of ENSO conditions is assigned for each required simulation, based on historical occurrence rates. (5) Kernel density functions (KDFs) are fitted to the observed 6-hourly cyclone locations (described in more detail later), one for each of the Neutral, El Niño and La Niña ENSO conditions. 6-Hourly observation locations are then simulated from the KDFs using ENSO- and location-dependent sampling rates. (6) The cyclone central pressure is simulated for each modeled 6-hourly observation location (described in more detail later). (7) Other cyclone parameters are sampled conditionally on the simulated central pressures: these being maximum sustained wind speed, RMW, cyclone propagation speed and direction. (8) For each simulated cyclone observation the surrounding wave field is simulated using three parametric models, and the wave conditions at the target location are recorded. (9) Using the simulated wave record at the target location, the frequency–magnitude relationship for extreme significant wave height is calculated. The significant wave height is defined as the average of the largest 1/3 of all wave heights in a wave record (Holthuijsen, 2007), and denoted H_s.

3.2. Cyclone climatology

SCMs can be divided into two classes: those that simulate cyclone tracks (e.g., Vickery et al., 2000b; Emanuel et al., 2006; Hall and

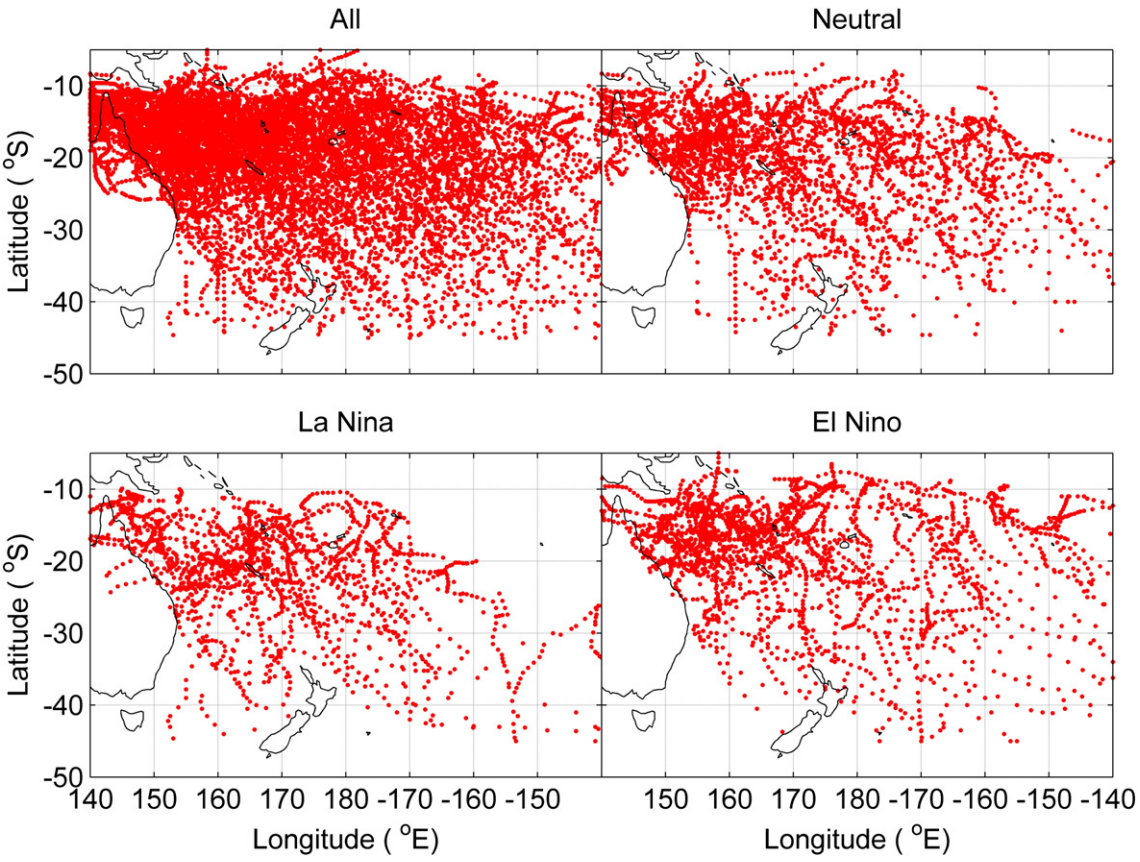

Fig. 1. Location of 6-hourly cyclone satellite observations 1969/70–2008/09 in the SW Pacific, stratified into ENSO-specific conditions.

Jewson, 2007; Rumpf et al., 2007) and so-called "local models" that do not (e.g., Russell, 1971; Georgiou et al., 1983; Vickery and Twisdale, 1995). Hall and Jewson (2008) found that track models simulated the landfall rate better than local models when small sections of coastline were considered, with correspondingly low historical local landfall rates. However, the reverse was also true that when larger coast sections were considered, there were more historical landfalls, and the local model scored better. Track model landfall accuracy comes with a price: they may suffer from bias due to inappropriate or missing statistical descriptions of physical processes (Hall and Jewson, 2008), and in regions with a high historical occurrence rate, track algorithms can struggle to correctly represent all of the historical variability. We chose to forgo the process of track simulation and potential associated bias, and have implemented a local model that is well-suited to model cyclone risk for the SW Pacific Ocean.

The local model was defined using a target window of 3° latitude (333 km) around the target location. The wave parametric models evaluate wave fields to ten times the RMW, of which the maximum value in the database was 204 km, leading to maximum wave field radius of >2000 km. However, the most extreme cyclone waves (the ones that are included in the extreme wave analysis) were generated by TCs much closer to the target location, as expected. Sensitivity tests showed little change in extreme cyclone hazard statistics using search radii ≥ 3° (333 km) showing that the wave fields important to the extreme-wave analysis are generated within this distance of the target location. This was true of regions that experience many TCs such as the Vanuatu

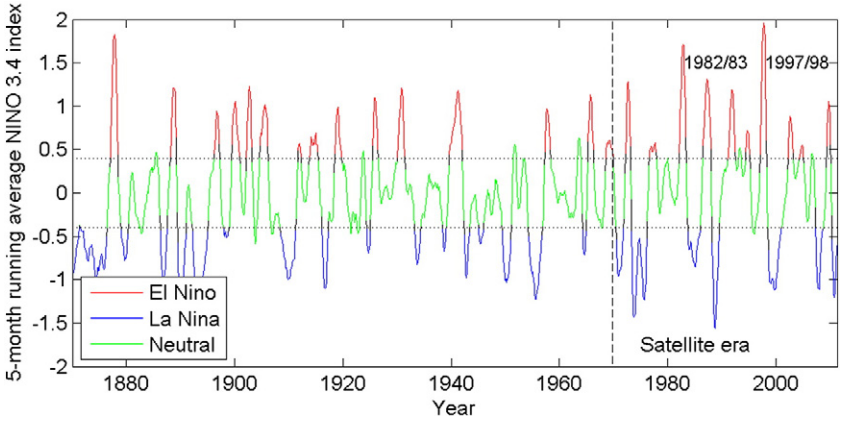

Fig. 2. Five-month running average of the NINO 3.4 sea-surface-temperature anomaly. ENSO classification follows Trenberth (1997) as described in the text.

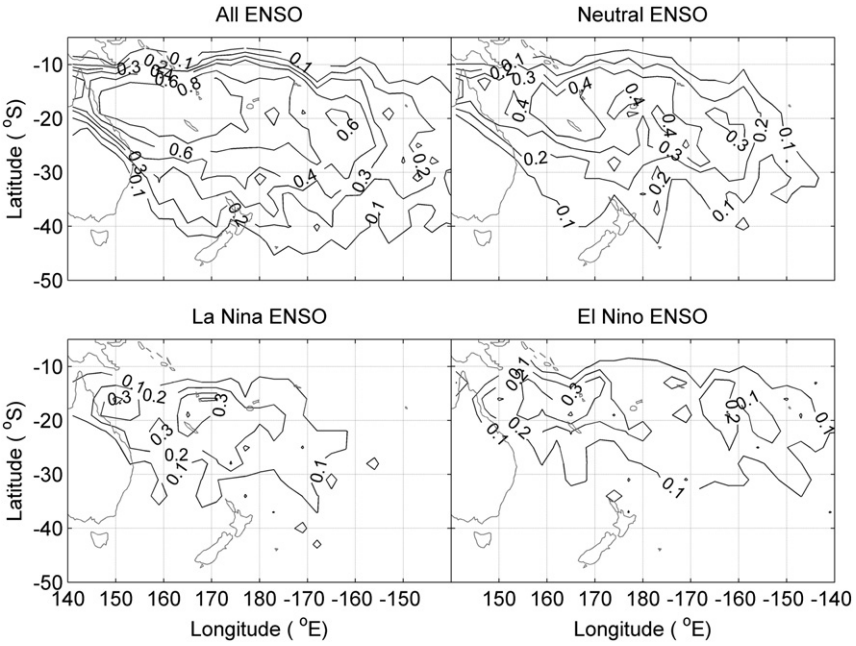

Fig. 3. ENSO-dependent average annual number of TCs in the SW Pacific Ocean in 3° × 3° boxes.

archipelago, and regions of relatively sparse TC activity such as French Polynesia. Using search radii ≤ 2° the extreme wave analysis becomes dominated by cyclones passing close to the target location, resulting in an over-prediction of the extreme wave climate.

Other SCMs have simulated cyclone genesis locations from their empirical spatial distribution, under the assumption that the spatial density distribution of genesis locations can be described as an inhomogeneous Poisson process model (e.g., Emanuel et al., 2006; Hall and Jewson, 2007; Rumpf et al., 2009). This model reflects the apparent absence of 'interaction' between the starting points of cyclones in the historical data. Statistical goodness-of-fit measures (Baddeley and Turner, 2005) show that cyclone genesis locations in the SW Pacific Ocean are also well described by an inhomogeneous Poisson point process model.

The SCM is based on random sampling of 6-hourly spaced satellite observations of cyclone parameters, from the best-tracks archive. This involves the assumption that the 6-hourly cyclone observation dataset is also well described as an inhomogeneous Poisson process model and can therefore be randomly sampled in time and space. However, observations from an individual cyclone are not randomly distributed. Once formed, the subsequent evolution of a cyclone depends on its previous properties of size, intensity and motion and so the individual observations within individual cyclones display 'interaction' and theoretically should not be modeled as a random Poisson process.

We suggest that when the cyclone dataset is combined to contain observations from many unique individual cyclones, over many seasons, then inter-cyclone randomness becomes locally more influential than intra-cyclone interactions. Under this assumption the distribution of cyclone parameters can be regarded as a random spatial point pattern. This assumption was tested using the inhomogeneous *K* function test for spatial point patterns within the Spatstat toolbox (Baddeley and Turner, 2005). The tests demonstrated that 6-hourly observations from individual cyclones display strong spatial clustering, as expected. Likewise, spatial clustering is significant when the entire SW Pacific-wide 6-hourly observation dataset is considered, due to regional influences. However, when the dataset was divided locally into search windows with side lengths of 3° latitude, the spatial point pattern of 6-hourly cyclone observations behaved as a random inhomogeneous Poisson process in most locations and could be randomly sampled accordingly. This finding also holds for ENSO-specific subsets of the observation locations. Therefore, 6-hourly observation locations were randomly simulated from the empirical distribution of local observations within a 3° latitude radius of the target location.

Nevertheless, in locations where there are few historical cyclones, such as in the north-east of the region, results could become too heavily influenced by central pressure data from only a few cyclones. For example, only one or two cyclones might have been observed within the 3° sampling radius around the target location (during the satellite era), and so the SCM would repeatedly sample those same cyclone observations, leading to a false representation of the long-term cyclone climate that presumably would include more variability if the observational record were longer. These low-resolution areas have been marked in the figures below.

3.3. Kernel density estimation of cyclone observation locations

An inhomogeneous Poisson process is characterized by its intensity function and the intensity value at a certain location indicates the frequency (or density) of points occurring at that location. Since we use 'intensity' to describe the strength of a cyclone, as defined by its central pressure, we will use 'density' to describe the intensity function of an inhomogeneous Poisson process, following Rumpf et al. (2010). If the true density function is unknown, as is the case in all 'real' data, it has to be estimated from the data (Rumpf et al., 2010). We used a two-dimensional Gaussian kernel density function to approximate the density function of the 6-hourly cyclone observation locations (Fig. 4). Kernel smoothing functions work to preserve the shape of the underlying dataset, providing an interpolator for missing data and allowing extrapolation beyond the original data range (Bowman and Azzalini, 1997). Kernel density functions have previously been used to estimate the genesis locations of TCs (e.g., Emanuel et al., 2006; Hall and Jewson, 2007; Rumpf et al., 2007, 2009, 2010). Cross-validation (Bowman and Azzalini, 1997) of the kernel-smoothed central pressure distribution suggested that the mean integrated square error remained relatively stable using Gaussian smoothing bandwidths of 1–4°. Therefore, because of its simplicity, normal optimal smoothing (Bowman and Azzalini, 1997) was used to determine the bandwidth for Gaussian kernel functions, leading to Gaussian kernel bandwidths of 3–4° in the zonal (longitudinal) direction and 1–1.5° in the meridional (latitudinal) direction.

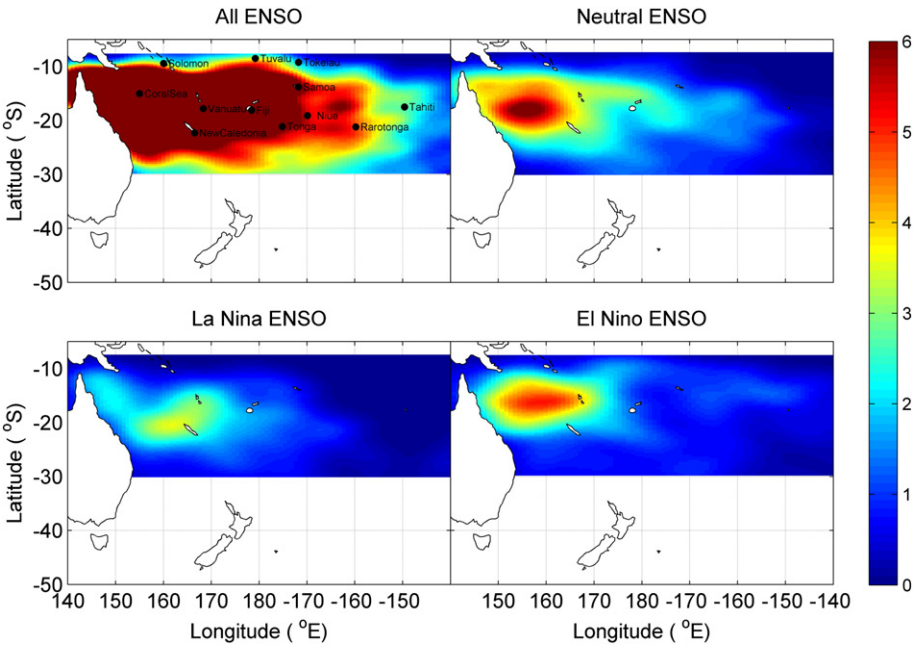

Fig. 4. ENSO-dependent Gaussian kernel-smoothed density functions of 6-hourly cyclone observations. Color scale shows the expected number of 6-hourly observations 1969/70–2008/09 per 1°-square of ocean.

3.4. Estimation of cyclone parameters

Like previous SCMs (Vickery et al., 2000b; Hall and Jewson, 2007; Rumpf et al., 2007; Emanuel and Jagger, 2010), the model relies on the assumption that cyclones located in similar areas of the observation window behave similarly. For each simulated 6-hourly observation location, the cyclone central pressure was sampled from nearby central pressure records (within a 3° sampling radius), using observations

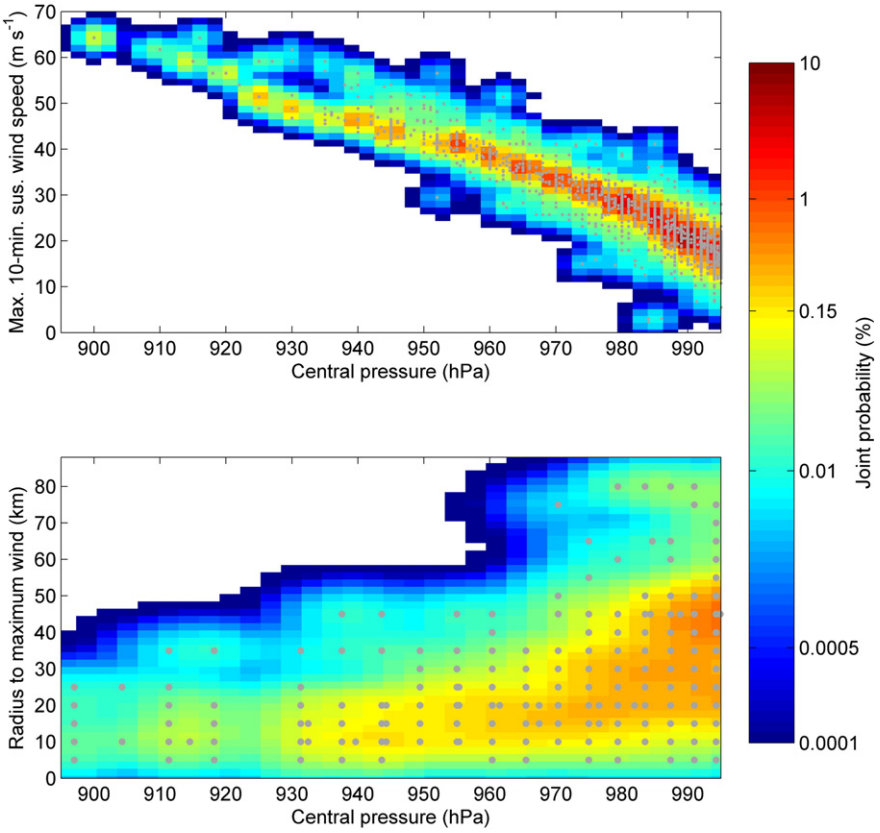

Fig. 5. Upper: Scatter plot of observed cyclone central pressure and maximum sustained wind speed (points), with shaded kernel-smoothed density function overlaid to represent the underlying probability mass. Lower: Scatter plot of observed cyclone central pressure and RMW. In these plots, the density functions have been normalized so that the joint probability sums to 100% over the sampling space, and joint-probabilities < 0.0001 are omitted from the plots, although they were included in the model.

specific to the ENSO condition being simulated. An empirical cumulative distribution function was constructed and then smoothed and extended by applying a one-dimensional variable-bandwidth kernel density estimator (Bowman and Azzalini, 1997). Central pressures were then simulated by randomly sampling the fitted kernel-smoothed density distribution.

Maximum sustained wind speed, RMW, cyclone propagation speed and direction were simulated using two-dimensional non-parametric kernel density estimators. This has the advantages of closely representing the underlying joint data distributions and also accounting for dependence between any two cyclone parameters. For example, Fig. 5 shows a kernel-smoothed density function (KDF) for cyclone central pressure and maximum sustained wind speed (top plot), and for cyclone central pressure and RMW (bottom plot). There is a strong dependence between central pressure and wind speed; intense cyclones with low central pressures tend to have more intense winds and vice versa. The dependence between central pressure and RMW is considerably weaker, but there is a tendency for the most intense cyclones of central pressure less than 970 hPa to have tighter vortices with RMW of less than 50 km. The two-dimensional KDFs form a sampling model for the probability mass of the joint observations and represent the natural variability between two parameters. Given a pre-sampled central pressure value (as described above), a maximum sustained wind speed is randomly sampled from the range of possible values, then the central pressure and wind speed are interpolated onto the KDF. Using Fig. 5 as an example, a central pressure of 989 hPa combined with a maximum sustained wind speed of 22 m s^{-1} is a relatively likely combination (~5% chance), whereas a combination of 905 hPa and 60 m s^{-1} is relatively rare, but still possible. Likewise, sampling from the lower KDF in Fig. 5 reproduces the observed tendency for smaller RMW at lower central pressure, and more scattered RMW at higher central pressure. Ultimately, given enough Monte Carlo samples, the sample space reproduces the KDF, sampling many "likely" combinations along with a few "rare" combinations. The strong relationship between central pressure and wind speed could have been represented parametrically with relatively high confidence, but this is not the case for central pressure and RMW, nor for other parameter combinations. The primary value of the KDF sampling method is to enable more scattered relationships to be replicated, such as that shown in the lower plot (Fig. 5). The parameter maximum sustained wind speed, RMW and cyclone propagation direction were simulated conditionally based on the pre-simulated central pressure, using KDFs, two of which are shown in Fig. 5. Cyclone propagation speed was sampled conditionally on pre-simulated cyclone propagation direction. Joint-probability kernels were constructed using data from the whole of the SW Pacific Ocean. Separate kernels were constructed and sampled for El Niño, La Niña and Neutral phases of the ENSO cycle.

In the Pacific, estimates of RMW are made from satellite measurements. For storms with clear eye structures, estimation of this quantity is relatively accurate, but for other storms it is less accurate (e.g. Hsu and Babin, 2005). Fortunately, uncertainty in RMW data does not affect the SCMs ability to predict the frequency–magnitude relationship of extreme wind or H_s. The maximum wave height predicted by the parametric wave models is highly sensitive to central pressure and associated wind speed, but it has a much weaker dependence on RMW. Although RMW is an important parameter when modeling the zone of influence of an individual TC (Vickery and Wadhera, 2008), during thousands of Monte Carlo simulations the extreme H_s field becomes dominated by direct strikes of the maximum wave height on the target location, and is relatively insensitive to RMW.

Fig. 6 compares the empirical and simulated CDFs for the five required cyclone parameters for 200,000 years of simulated cyclones within 3°-latitude radius of Tonga, illustrating a good visual match between the individual empirical and simulated parameter distributions. Thus, the distribution of individual parameters has been preserved at the same time as accounting for the joint distribution between parameters.

3.5. Simulate wave hazard

Having simulated many years of cyclone parameters inside the target window, the next step was to simulate the associated ocean wave field for each set of cyclone parameters. Complex dynamic models exist for simulating cyclone wave fields (e.g., Cardone et al., 1976; Skamarock et al., 2008; Warner et al., 1978; Young, 1988), but since many thousands of simulations are required to return robust extreme-value statistics, these dynamic models are too computationally expensive for our Monte Carlo simulation approach. Instead, parametric models offer a means to rapidly simulate the wave (also wind and atmospheric pressure) field for each set of simulated cyclone parameters.

TCs are convectively-driven wind vortices (Sinclair, 2002). Their symmetry means they can be successfully modeled using relatively simple analytical models to describe the sea level pressure and wind profile distribution (e.g., Holland, 1980), and subsequent momentum transfer into sea waves (Ross, 1976; Cooper, 1988; Young, 1988). These analytical models require only a few descriptive parameters and are consequently named 'parametric models'. Cyclone parametric models are strictly applicable to storms only with constant wind field parameters, linear track, and over deep water far from land. Real TCs are constantly evolving due to the changing ocean and atmospheric conditions that form and maintain them, leading to evolution of the wind and wave field as the TC changes in intensity, translation speed and direction. Close to land, the wind and wave fields interact with the landmass and seabed to cause deviations from the parametric form. Fortunately however, many deep-ocean TCs can be approximated using parametric models (e.g. Young, 1988; Chu and Wang, 1998; Casson and Coles, 2000; Kossin and Camargo, 2009). A caveat is that the symmetric vortex structure of cyclones changes as they move southward out of the generation zone (5–20°S) toward higher latitudes, where they transform into extratropical mid-latitude storms. In the SW Pacific Ocean the onset of this transformation begins at about 20°S and from 25°S poleward the storm has all the characteristics of a mid-latitude storm (Sinclair, 2002). Thus the parametric models will be increasingly less accurate south of 25°S. There is drop-off in both the occurrence density and intensity of cyclones southward of 25°S, and we have plotted results as far south as 30°S to illustrate this transition.

The parametric models of Ross (1976), Cooper (1988) and Young (1988) were used. The Ross and Cooper models use analytical wind and wave solutions fitted to cyclone observations, while the Young model uses mapped wave fields from dynamic wave model simulations of a range of cyclone scenarios. All three parametric models were verified against buoy measurements of cyclone waves. Rather than rely on just one model, the comparison of three parametric models highlights the variability in results arising from different model parameterizations.

For each simulated cyclone wave field, the wave field experienced at the target location was determined by assuming the cyclone would remain on its present track for the following 6-hour observation period. The maximum wave statistics along that track of 6-hour duration were recorded at the target location. Only a proportion of the simulated cyclones actually impact the target location.

A count-back technique was used to calculate frequency magnitude relationships for extreme H_s (e.g., Hawkes et al., 2002). This involves simulating cyclones for (at least) 10 times the number of years of the required maximum average recurrence interval, then sorting the wave heights and counting back to assign the occurrence likelihood. For example, if 1000 annual maxima are simulated, then the 10th-highest value represents the 100-year average recurrence interval. Confidence intervals can be generated around a median "best-fit" estimate, by undertaking sufficient Monte Carlo simulations to generate around 200 frequency–magnitude relationships, whose statistics produce median and 95% tolerance interval estimates at each return probability.

Presently the SCM includes no topographic wind or wave sheltering effects, so results are strictly valid only for deep water in open ocean. The frequency–magnitude curves for H_s include only cyclone waves,

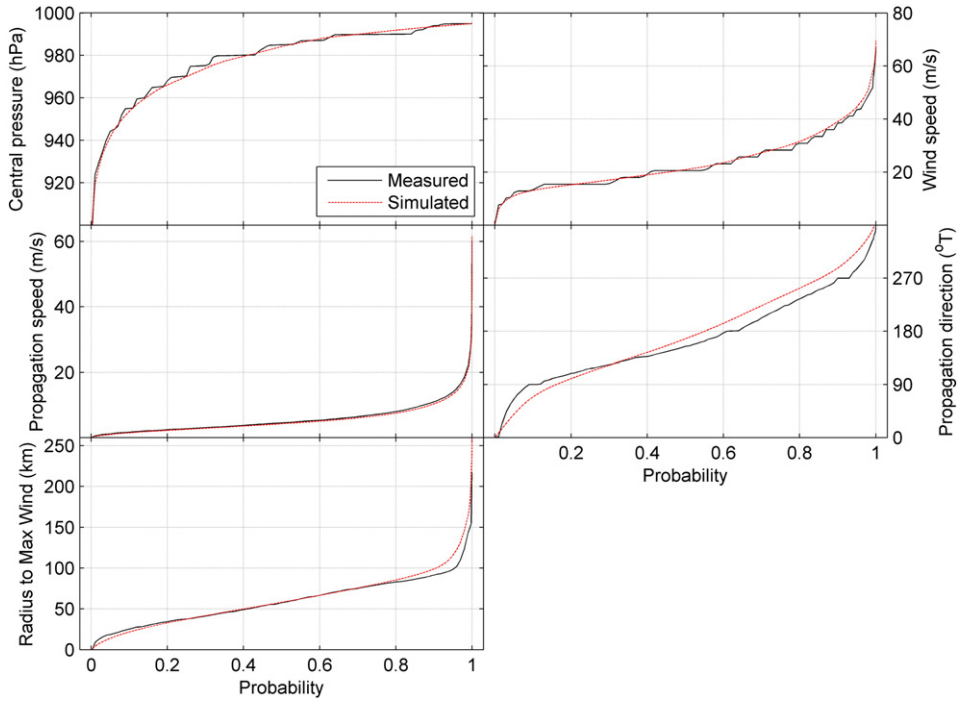

Fig. 6. Comparison of empirical and simulated cumulative distribution functions for the five simulated cyclone parameters, for 200,000 years of simulated cyclones within 3° of Tonga.

and not swell waves emanating from high-latitude storms, or general meteorological and oceanographic conditions, such as the trade winds for example. Swell waves are expected to modify the high-frequency end of the frequency–magnitude curve, requiring a mixed model. Estimated breaking wave heights from a mid-latitude storm that caused widespread wave-driven inundation of Pacific Islands in December 2008 were ≤6 m except at Wake Island where they were estimated at 9 m (Hoeke et al., 2013). Simulated H_s from the SCM exceeds 6 m at AEP ≤ 1/10 (Table 1). In the absence of a formal comparison from a mixed model, we infer that the SCM frequency–magnitude results are reasonable for AEP ≤ 1/10 approximately.

4. Results

4.1. Extreme cyclone significant wave height in the SW Pacific Ocean

Fig. 7 shows the example frequency–magnitude plots for extreme cyclone H_s, for the three parametric wave models, at a deep-ocean location in the Vanuatu archipelago, one of the most active areas for TC development and related impacts in the SW Pacific basin (Diamond et al., 2013). Fig. 7 also shows the confidence intervals for the modeled extreme-value curve: for clarity shown only for the Young (1988) model. This is a typical output from the SCM, which also produces similar information for wave period or inverse-barometer cyclone storm surge, or joint-statistics for joint-probability analyses of wave height and period or storm surge and wave height, for example. The SCM is thus used to quantify the magnitude of the cyclone hazard in terms of its occurrence likelihood: shown in Fig. 7 for H_s in terms of annual exceedance probability (AEP). AEP is related to the average recurrence interval (ARI), a term used to describe the average interval between events that equal or exceed a given magnitude (over a long period of time and many exceedances): AEP = $1-e^{\frac{-1}{ARI}}$, which approximates to AEP = 1/ARI for ARI ≥ 10 years.

The three parametric models produce different results, owing to the different empirical datasets used in their derivation, and to different analytical (Ross and Cooper) and dynamic model (Young) solutions (Fig. 7, Table 1). For low-frequency events, the Ross model predicted the largest wave conditions and the Cooper model the smallest. The difference between the Ross and Cooper model was commonly H_s = ~1.8 m and up to H_s = 3 m for AEP = 1/50, depending on location.

Although H_s magnitude differed, the spatial distribution pattern of H_s was similar for the three parametric models, being governed by the

Table 1
Median significant wave height (m) during TCs associated with annual exceedance probabilities (AEPs) of 0.1, 0.02 and 0.01 at selected SW Pacific inhabited locations, for all ENSO conditions, using three parametric models (C = Cooper (1988), Y = Young (1988), R = Ross (1976)).

Location	0.1 AEP			0.02 AEP			0.01 AEP		
	C	Y	R	C	Y	R	C	Y	R
Vanuatu (168.3°E, 17.8°S)	8.2	7.9	7.7	10.4	10.8	11.1	11.2	12.0	12.5
Noumea (New Caledonia 166.5°E, 22.3°S)	7.6	7.9	8.8	10.0	10.7	12.7	11.0	11.6	14.4
Tuvalu (179.2°E, 8.5°S)	6.0	5.0	6.4	7.4	8.0	8.9	8.2	9.3	10.1
Fiji (178.4°E, 18.1°S)	8.4	7.6	8.4	11.2	10.8	12.0	12.0	11.6	13.2
Tokelau (171.8°W, 9.2°S)	7.9	7.8	8.0	10.0	11.2	11.5	10.8	12.1	12.9
Samoa (171.8°W, 13.8°S)	7.7	7.9	8.9	10.6	11.4	13.7	11.6	12.6	15.3
Niue (169.9°W, 19.1°S)	7.7	7.8	8.2	10.1	11.3	12.5	11.1	12.5	14.4
Rarotonga (159.8°W, 21.2°S)	7.9	7.0	9.1	9.9	9.8	12.5	11.0	10.8	13.4
Tahiti (149.6°W, 17.5°S)	8.3	8.8	8.6	11.0	12.0	12.5	12.0	13.2	13.7
Honiara (Solomon Islands 160.0°E, 9.4°S)	7.0	6.9	6.1	8.7	10.0	8.6	9.2	11.1	9.6
Coral Sea (155.0°E, 15.0°S)	7.1	7.0	8.1	9.1	9.9	11.4	9.9	11.2	12.7
Tonga (175.2°W, 21.1°S)	7.7	7.1	8.6	9.6	10.2	12.0	10.5	11.3	13.2

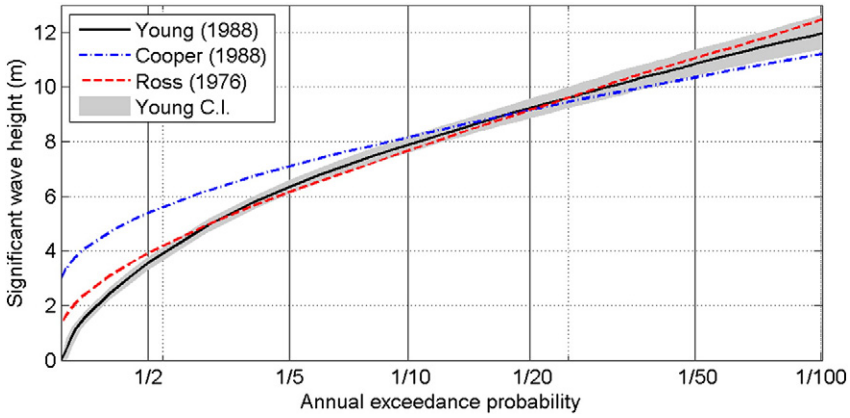

Fig. 7. Significant wave height frequency–magnitude relationships for Vanuatu (17.8°S, 168.3°E), calculated using three cyclone parametric models. The shading represents 95% confidence intervals, for the Young (1988) model only.

historical distribution of observed cyclones. Rather than select one parametric model, the three models were averaged to examine the spatial variability of H_s in the SW Pacific Ocean (Fig. 8). Fig. 8 was generated by predicting extreme wave heights in a grid at 5° intervals before interpolating and smoothing between. At AEP = 1/50 simulated H_s ranged from a low of about 7 m to a maximum of about 15 m, with a median of approximately 10 m. Similar spatial distribution patterns were observed for other AEP (not shown), but the magnitude differed; for example H_s medians were ~11 m for AEP = 1/100 and ~7.5 m for AEP = 1/10. The most extreme waves were predicted to occur in the latitude band of approximately 15 to 25°S, reflecting favorable atmospheric and sea surface temperature (SST) conditions for intense TCs.

4.2. Modeling climate variability — the effect of ENSO

The effect of ENSO variability on extreme H_s was explored using the SCM. Fig. 9 demonstrates the effect of ENSO on the extreme H_s frequency–magnitude curves for Vanuatu. The extreme H_s climate is smallest during La Niña, and largest during El Niño conditions, with Neutral conditions lying between. The frequency–magnitude curve for Neutral conditions is similar to the ENSO-averaged curve. The La Niña curve lies outside the 95% confidence interval of the ENSO-averaged curve while the El Niño curve lies outside or near the upper confidence interval. These patterns of ENSO influence were typical of most locations (e.g. Table 2).

Fig. 10 illustrates the spatial variability in extreme H_s for La Niña, El Niño and Neutral ENSO conditions, corresponding to an AEP of 1/50, for comparison with the ENSO-averaged simulation in Fig. 8. Extreme H_s was predicted to be higher across the entire region during El Niño compared with La Niña and Neutral conditions. During El Niño the most extreme cyclone wave climate was predicted to occur in the east of the region, in the ocean between and adjacent to Samoa, Niue and Rarotonga. Conversely, the extreme wave climate was much lower in the east during La Niña, with the largest wave heights occurring west of Tonga, affecting Fiji, Vanuatu, New Caledonia and the Coral Sea. In the Vanuatu archipelago, extreme H_s corresponding to AEP = 1/50 was ~1.5 m lower during La Niña than those occurring during El Niño conditions (e.g. Fig. 9). Whereas the extreme H_s magnitude was predicted to be larger in the west during La Niña and in the east during El Niño, a more balanced zonal distribution was predicted for Neutral conditions. During Neutral conditions a heightened H_s hazard was predicted near the coast of Australia centered near 150°E, 23°S. Otherwise, Neutral spatial distribution patterns had features common to both the El Niño and La Niña specific simulations, likely reflecting both transitions that occur between ENSO conditions and also an imperfect categorization of the cyclone observations into separate ENSO phases using the NINO 3.4 index.

The predicted spatial patterns of extreme H_s reflect patterns of both cyclone observational density and also cyclone intensity (low central pressure). The different spatial distributions of extreme H_s between La Niña and El Niño (Fig. 10) are not obvious in the spatial distribution of

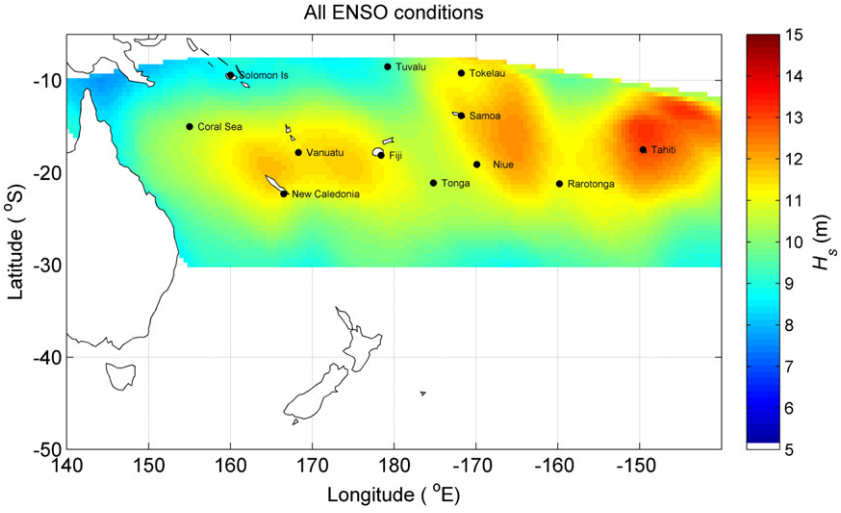

Fig. 8. Significant wave height (m) associated with an annual exceedance probability of 1/50, calculated from the average of three cyclone parametric models, for all ENSO conditions. Note the presence of three high-intensity regions (HIRs).

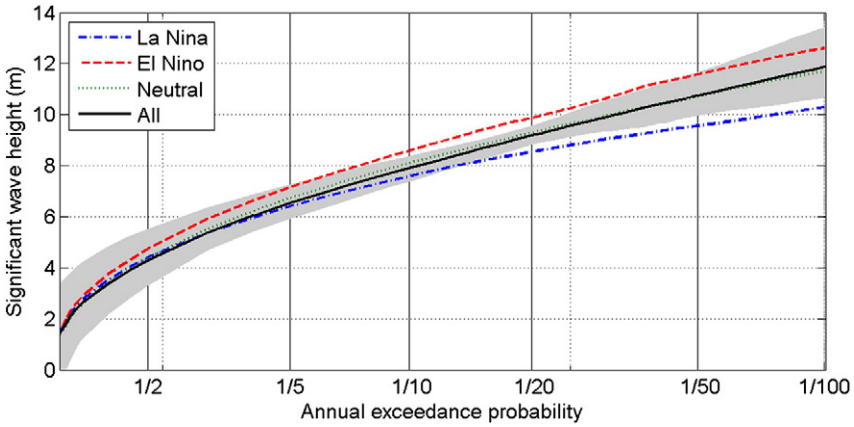

Fig. 9. Median (50th percentile) significant wave height frequency–magnitude relationships for Vanuatu (17.8°S, 168.3°E), calculated for various ENSO conditions from the average of three cyclone parametric models. Gray shading spans minimum 2.5% and maximum 97.5% confidence intervals from three parametric models, for 'all' ENSO conditions only.

cyclone observation density (Figs. 3, 4), although the shift of cyclone tracks to the north-east of the region during El Niño can be seen in Fig. 1. Instead, the spatial distribution of extreme H_s more closely matches that of local propensity for intense cyclones, represented in Fig. 11 for La Niña and El Niño conditions. Fig. 11 shows a kernel-smoothed density function that models locally-averaged central-pressure anomaly, constructed by applying the kernel smoothing functions derived for cyclone observation densities (Fig. 4) to the central pressure anomalies (defined as 995 hPa − central pressure). The spatial distributions of locally-averaged central-pressure anomaly are influenced both by the occurrence density and the central-pressure anomaly 'intensity', with ENSO having a pronounced influence. During La Niña conditions the most intense cyclones were restricted mainly to the west of the International Dateline, with a high-intensity 'tongue' extending southeast past the North Island of New Zealand, and a weaker tongue extending from the Coral Sea southward along the east coast of Australia. During El Niño, higher average cyclone intensity occurred over a broader zonal band that extends zonally northward of about 25°S, and is markedly more intense to the east of the International Dateline.

When integrated over the 40-year observation period containing several ENSO cycles (e.g. Fig. 2), the extreme H_s spatial distribution included three high-intensity regions (HIRs), the first positioned west of 175°W and the second two positioned east of 175°W, with a HIR lying east of Niue, Samoa and Tokelau, and another HIR centered near Tahiti (Fig. 8). Fig. 11 indicates that the western HIR results from the occurrences of relatively high intensity cyclones, present during all ENSO conditions (including Neutral conditions, not shown). In contrast, the HIR east of 175°W was instead driven by a few relatively intense cyclones in the east of the region that occurred primarily during El Niño conditions, and to a lesser extent also in conditions here classified as Neutral (not shown). The easternmost HIR centered on Tahiti was heavily influenced by intense TCs during the strong 1982/83 and 1997/98 El Niño seasons, as discussed later. When the SCM is used to simulate many thousands of years including many ENSO cycles, this leads to a prediction of greatest extreme H_s hazard in the east of the region despite a relatively low long-term cyclone occurrence rate here. Thus, cyclone hazard is strongly influenced by spatial intensity distribution and not just genesis and observation location and frequency; SCMs should account for both when quantifying ENSO influence on cyclone hazard.

4.3. Modeling climate change

Climate change is expected to affect the frequency and intensity of tropical cyclones. Projections in the South Pacific generally indicate an increase in the intensity of the most intense cyclones, along with a reduction in the total number of cyclones, although with some uncertainty (Knutson et al. (2010); Walsh et al. (2012)). The SCM allows us to explore the effects of climate change on extreme wave climate by perturbing the intensity and occurrence rate of cyclones to represent the effects of climate change, relative to recent historical observations. Following Knutson et al. (2010) and Walsh et al. (2012) the following three scenarios were simulated: (1) a 10% increase in the intensity of category 4 and 5 cyclones (those cyclones with a simulated maximum 10-minute-sustained wind speed of ≥160 km/h); (2) a 10% increase in the intensity of category 4 and 5 cyclones and a 10% reduction in the average number of cyclones (of all categories), and (3) a 20%

Table 2
Median significant wave height (m) during TCs with an annual exceedance probability of 0.01 (100-year ARI), at SW Pacific islands, for various ENSO and climate-change simulations. Results are from the average of three parametric models.

Location	ENSO conditions				Climate-change simulations		
	All	El Niño	La Niña	Neutral	+10% 0%	+10% −10%	+20% −20%
Vanuatu (168.3°E, 17.8°S)	11.9	12.6	10.3	11.7	12.3	12.2	12.7
Noumea (New Caledonia 166.5°E, 22.3°S)	12.3	13.9	11.1	11.6	12.8	12.7	12.8
Tuvalu (179.2°E, 8.5°S)	9.2	11.5	8.1	7.4	9.1	9.4	9.5
Fiji (178.4°E, 18.1°S)	12.3	13.2	10.5	9.7	13.0	12.9	13.2
Tokelau (171.8°W, 9.2°S)	11.9	13.4	7.8	10.9	12.7	12.3	12.5
Samoa (171.8°W, 13.8°S)	13.2	13.9	8.2	11.4	13.8	13.8	14.2
Niue (169.9°W, 19.1°S)	12.7	13.7	8.2	11.2	13.0	12.9	13.6
Rarotonga (159.8°W, 21.2°S)	11.7	14.4	9.6	10.8	12.2	12.1	12.5
Tahiti (149.6°W, 17.5°S)	13.0	14.0	N/A	12.6	13.5	13.4	14.1
Honiara (Solomon Islands 160.0°E, 9.4°S)	10.0	10.4	9.3	9.6	10.1	10.2	10.1
Coral Sea (155.0°E, 15.0°S)	11.3	12.4	10.3	10.6	11.4	11.5	11.5
Tonga (175.2°W, 21.1°S)	11.7	13.4	10.0	11.1	12.0	11.8	12.2

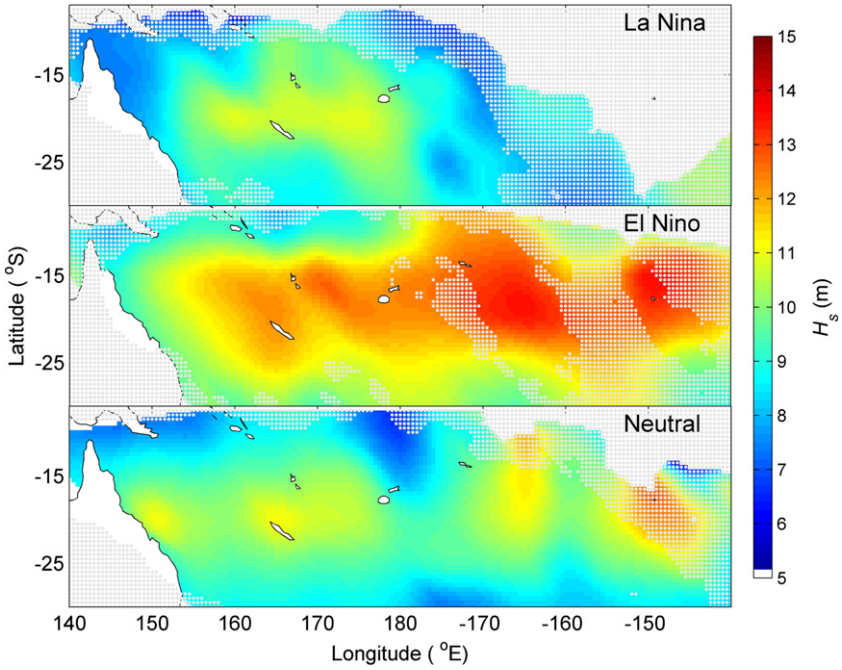

Fig. 10. Significant wave height (m) for various ENSO conditions, for an annual exceedance probability of 1/50, calculated from the average of three cyclone parametric models. The light-gray mask shows locations where there were observations from less than 6 unique cyclones within a 3° radius: indicating lower confidence in the results in these areas.

increase in the intensity of category 4 and 5 cyclones and a 20% reduction in the average number of cyclones. A typical example of the climate change simulation results is shown in Fig. 12 for Vanuatu. Climate change effects on extreme H_s are indistinguishable from present-day conditions for more frequently occurring moderate-intensity cyclones, and only at annual exceedance probabilities of 1/20 or less do the climate change effects on H_s become distinguishable. Climate change effects on extreme H_s are considerably less noticeable than the effects of ENSO climate variability (compare Figs. 9 and 12). It is therefore speculated that the climate change effects on the SW Pacific wave climate will be primarily mediated by the changes in the ENSO characteristics under greenhouse warming.

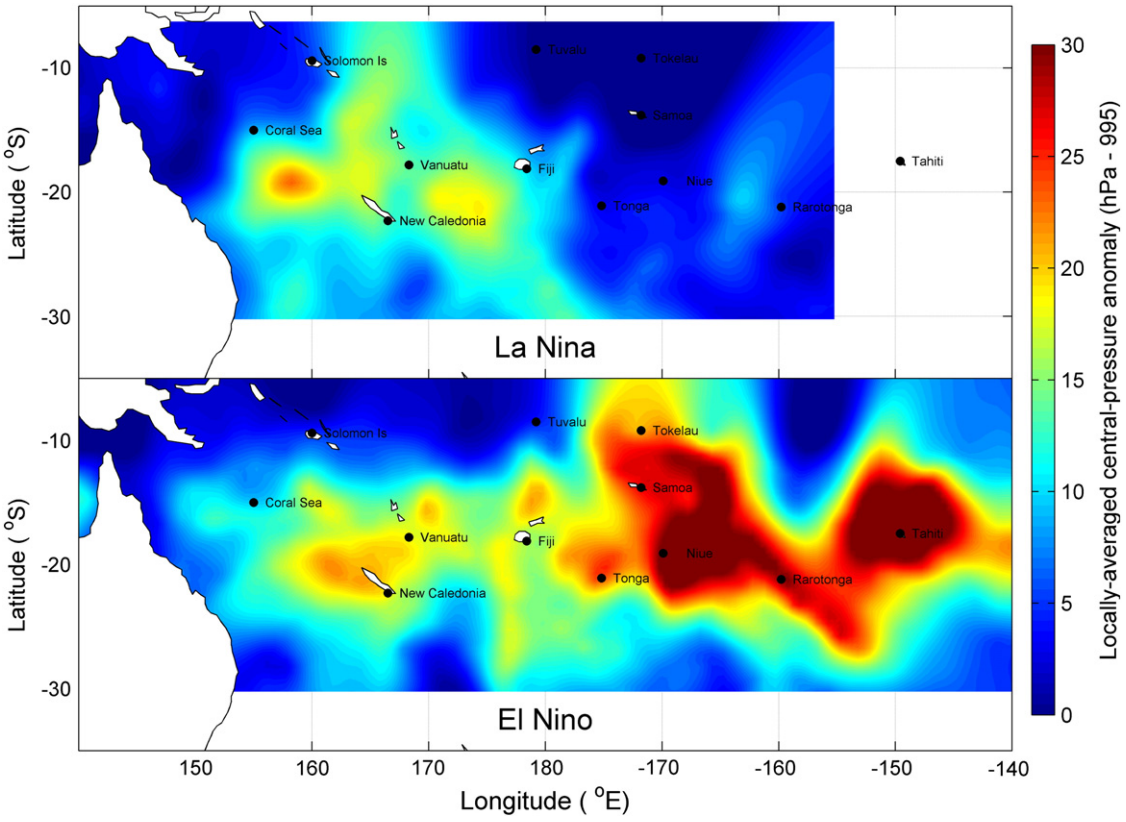

Fig. 11. Kernel-smoothed density function of cyclone central pressure anomaly (995 − central pressure in hectoPascals) for La Niña and El Niño conditions. La Niña shading map is truncated at 165°E due to lack of data further east.

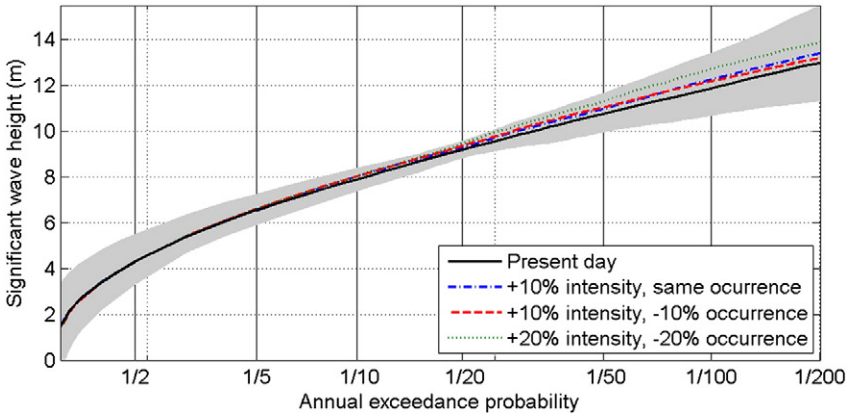

Fig. 12. Median (50th percentile) significant wave height frequency–magnitude relationships for Vanuatu (17.8°S, 168.3°E), calculated for various climate change options from the average of three cyclone parametric models. Gray shading spans minimum 2.5% and maximum 97.5% confidence intervals from three parametric models, for present-day conditions only. Intensity changes apply to category 4 and 5 cyclones, while occurrence changes apply to the total number of cyclones.

5. Discussion

In the vicinity of French Polynesia the satellite-era cyclone observations are dominated, in terms of frequency and intensity, by the 1982/83 and 1997/98 cyclone seasons. These extreme El Niño events lead to predictions of the highest long-term extreme wave climate in that region, being responsible for the high-intensity region centered near Tahiti (Fig. 8).

The satellite era spans a period in which the intensity and number of El Niño events were high compared to much of the preceding century (Fig. 2), correlating with suggestions of an amplification of the ENSO signal in tropical Pacific sea-level observations since 1970 (Becker et al., 2012). The satellite era also spans a positive phase (1978–1998) of the Interdecadal Pacific Oscillation (IPO), which is a significant source of climate variation on decadal time scales throughout the SW Pacific region and also modulates interannual ENSO climate variability over the region (Salinger et al., 2001), including the position of the SPCZ that strongly influences regional TC formation and propagation (Folland et al., 2002; Widlansky et al., 2011). Strong El Niño is more prevalent during positive IPO.

Thus the SCM, based on modern satellite-era data, potentially overrepresents the frequency of high-intensity cyclones in the northeast quadrant of the SW Pacific relative to historical conditions. However, Santoso et al. (2013) suggest that climate change will substantially increase the occurrences of El Niño events that feature prominent eastward propagation characteristics, like the 1982/83 and 1997/98 events for example. Furthermore, Cai et al. (2014) presented climate modeling evidence for a doubling in the occurrences of extreme El Niño in the future in response to greenhouse warming. Hence patterns of intense cyclones in the east of the region are expected to become more prevalent, reinforcing the pattern of higher extreme cyclone wave hazard east of the Dateline (Fig. 8).

Despite a propensity for more intense cyclones on average over the long term, regions east of the Dateline have respite during La Niña conditions, whereas for the Vanuatu archipelago the cyclone hazard remains high regardless of ENSO phase (see also Diamond et al. (2013)).

5.1. Climate change versus climate variability

The predicted change in the median extreme H_s is relatively small for all three simulated climate change scenarios, and all are within the 95% confidence intervals of the present-day estimate. In contrast, ENSO climate variability had a much greater influence on extreme H_s (Fig. 9) than predicted future moderate changes in either the intensity or frequency of cyclone events (Fig. 12). The findings are similar to those of McInnes et al. (2014) who predicted little change in extreme TC storm surges at Fiji due to projected climate change, for AEP ≥ 1/100. The results support other studies demonstrating the pronounced influence of climate variability on cyclone and track characteristics (Vincent, 1994; Salinger et al., 1995; Folland et al., 2002; Terry and Gienko, 2010; Diamond et al., 2013), and support suggestions that such climate variability will remain a much more dominant feature of temporal patterns in the South Pacific Ocean than possibly evolving changes in long-term average cyclone activity resulting from climate change (Terry and Gienko, 2010).

The SCM results are important in context of uncertainty in climate change in the Pacific, given recent evidence that movement of the SPCZ will be more extreme in a warmer climate and extreme El Niño occurrences could approximately double (Cai et al., 2014). The SCM suggests that such climate change effects will result in a more extreme wave climate over the entire SW Pacific, and particularly in the east of the region, and that this change will arise through ENSO variability rather than climate mean trends. Although not specifically mapped here, since the wave parametric models in the SCM reflect wind speed, which is strongly related to cyclone central pressure, this implies a more extreme cyclone wind and storm surge climate in future also.

6. Conclusions

Large waves and wave amplification from TCs are a significant natural hazard for inhabitants of SW Pacific islands. This paper describes a new SCM and its use to quantify the extreme significant wave heights from TC activity in the SW Pacific, for the first time. The model samples non-parametrically from joint empirical density functions that preserve the dependencies between the key cyclone parameters required for running cyclone parametric models, such as central pressure, wind speed and RMW.

The largest extreme significant wave heights occurred within latitude band 15–25°S. The median extreme significant wave heights across the entire SW Pacific Ocean were 7.5, 10 and 11 m for annual exceedance probabilities of 1/10, 1/50 and 1/100 respectively. Maximum significant wave heights in the region were approximately 1.5 times these values. Extreme wave heights for selected inhabited locations were tabulated at AEP = 1/10, 1/50 and 1/100 for the three parametric models during all ENSO conditions (Table 1), and at AEP = 1/100 for various ENSO and climate-change scenarios (Table 2).

The El Niño-Southern Oscillation had a pronounced influence on both the strength and the spatial distribution of cyclone wave hazard. West of the International Dateline, in the region of the Vanuatu archipelago, the extreme cyclone wave climate was high during all phases of the ENSO cycle. Eastward of the Dateline, the cyclone observation rate dropped and the cyclone hazard was relatively low during La

Niña. However, cyclone observations east of the Dateline tended to be associated with El Niño conditions and were more likely to be intense, leading to the largest extreme-wave climate here when averaged over thousands of years of simulations.

A few intense cyclones can dominate the extreme wave climate, hence the spatial distribution of central pressure anomaly had more influence on extreme wave hazard than spatial patterns of cyclone observation density; thus SCMs should account for both when quantifying ENSO influence on cyclone hazard.

Simulated climate change cyclone intensity increases of 10–20% along with 10–20% reduction in number of cyclones, indicated relatively subtle increases in extreme significant wave heights for low-occurrence probabilities of 1/20 or less. ENSO climate variability had a much greater influence on extreme significant wave height than predicted future moderate changes in either the intensity or frequency of cyclone events. The SW Pacific Ocean extreme cyclone wave hazard is considerably larger during El Niño conditions, and the occurrence of two extreme El Niño events in the satellite observation era (1982/83 and 1997/98) led to predictions of the highest extreme-wave climate in the east of the region. This suggests that any future climate change influences on the frequency and intensity of such strong El Niño events will be a key influence on the regional extreme wave climate. Recent model results strongly suggest that the frequency of extreme El Nino is likely to double under greenhouse warming. Such a change would have profound impacts on the wave climate of the SW Pacific, especially when superimposed onto long-term sea-level rise.

Acknowledgments

Many thanks to Dr Andrew Lorrey and Dr Nicolas Fauchereau for valuable comments during manuscript preparation. We are grateful for the insightful comments of an anonymous reviewer that helped to improve the manuscript. The SCM was originally developed as part of the study “Climate change impacts on coastal inundation at Oneroa village, Mangaia. A Geospatial Framework for Climate Change Adaptation in the Coastal Zone of Mangaia, Cook Islands. Prepared for Ministry of Infrastructure and Planning, Cook Islands”, that was funded as part of the Pacific Adaptation to Climate Change (PACC) project administered by the Secretariat of the Pacific Regional Environment Programme (SPREP) (Stephens and Ramsay, 2012). Subsequent model refinement and manuscript preparation was undertaken in NIWA's Forecasting Coastal Hazards projects HAFS1303 and HAFS1403, and NIWA Pacific Rim National Centre core funded project PRAS1401, funded by the New Zealand Ministry of Business, Innovation and Employment (MBIE). Cyclone observations were downloaded from the International Best Track Archive for Climate Stewardship (IBTrACS) http://www.ncdc.noaa.gov/ibtracs. The NINO 3.4 sea-surface-temperature anomaly index was obtained from the Hadley Centre Sea Ice and Sea Surface Temperature data set (HadISST) www.metoffice.gov.uk/hadobs.

References

Alves, J., Young, I.R., 2003. On estimating extreme wave heights using combined Geosat, Topex/Poseidon and ERS-1 altimeter data. Appl. Ocean Res. 25 (4), 167–186.
Baddeley, A., Turner, R., 2005. Spatstat: an R package for analyzing spatial point patterns. J. Stat. Softw. 12 (6), 1–42.
Becker, M., et al., 2012. Sea level variations at tropical Pacific islands since 1950. Glob. Planet. Chang. 80–81, 85–98.
Bowman, A.W., Azzalini, A., 1997. Applied smoothing techniques for data analysis. The kernel approach with S-Plus illustrations. Oxford Statistical Science SeriesOxford University Press, Clarendon (193 pp.).
Bretschneider, C.L., 1990. Tropical cyclones. In: Herbich, J.B., Bretschneider, C.L. (Eds.), Handbook of Coastal & Ocean Engineering. Gulf Pub. Co., Houston, pp. 249–303.
Cai, W., et al., 2014. Increasing frequency of extreme El Nino events due to greenhouse warming. Nat. Clim. Chang. 4 (2), 111–116.
Cardone, V.J., Pierson, W.J., Ward, E.G., 1976. Hindcasting the directional spectra of hurricane-generated waves. J. Pet. Technol. 28 (4), 385–394.
Casson, E., Coles, S., 2000. Simulation and extremal analysis of hurricane events. J. R. Stat. Soc.: Ser. C: Appl. Stat. 49, 227–245.
Challenor, P.G., Foale, S., Webb, D.J., 1990. Seasonal changes in the global wave climate measured by the GEOSAT altimeter. Int. J. Remote Sens. 11, 2205–2213.
Chand, S.S., Walsh, K.J.E., 2009. Tropical cyclone activity in the Fiji region: spatial patterns and relationship to large-scale circulation. J. Clim. 22 (14), 3877–3893.
Chand, S.S., Walsh, K.J.E., 2010. The influence of the Madden–Julian oscillation on tropical cyclone activity in the Fiji region. J. Clim. 23 (4), 868–886.
Chouinard, L.E., Liu, C., Cooper, C.K., 1997. Model for severity of hurricanes in Gulf of Mexico. J. Waterw. Port Coast. Ocean Eng. ASCE 123 (3), 120–129.
Chu, P.S., Wang, J.X., 1998. Modeling return periods of tropical cyclone intensities in the vicinity of Hawaii. J. Appl. Meteorol. 37 (9), 951–960.
Church, J.A., Hunter, J.R., McInnes, K.L., White, N.J., 2006. Sea-level rise around the Australian coastline and the changing frequency of extreme sea-level events. Aust. Meteorol. Mag. 55, 253–260.
Coles, S., 2001. An Introduction to Statistical Modeling of Extreme Values. Springer, London; New York (208 pp.).
Cooper, C.K., 1988. Parametric models of hurricane-generated winds, waves, and currents in deep water. Proceedings of 20th Offshore Technology Conference, pp. 475–484 (Houston, Texas, USA).
Daniel, P., Haie, B., Aubail, X., 2009. Operational forecasting of tropical cyclones storm surges at Meteo-France. Mar. Geod. 32 (2), 233–242.
Diamond, H.J., Lorrey, A.M., Knapp, K.R., Levinson, D.H., 2012. Development of an enhanced tropical cyclone tracks database for the Southwest Pacific from 1840 to 2010. Int. J. Climatol. 32 (14), 2240–2250.
Diamond, H.J., Lorrey, A.M., Renwick, J.A., 2013. A Southwest Pacific tropical cyclone climatology and linkages to the El Nino-Southern Oscillation. J. Clim. 26 (1), 3–25.
Emanuel, K., Jagger, T., 2010. On estimating hurricane return periods. J. Appl. Meteorol. Climatol. 49 (5), 837–844.
Emanuel, K., Ravela, S., Vivant, E., Risi, C., 2006. A statistical deterministic approach to hurricane risk assessment. Bull. Am. Meteorol. Soc. 87 (3), 299–312.
Folland, C.K., Renwick, J.A., Salinger, M.J., Mullan, A.B., 2002. Relative influences of the Interdecadal Pacific Oscillation and ENSO on the South Pacific Convergence Zone. Geophys. Res. Lett. 29 (13), 1643.
Georgiou, P.N., Davenport, A.G., Vickery, B.J., 1983. Design wind speeds in regions dominated by tropical cyclones. J. Wind Eng. Ind. Aerodyn. 13, 139–152.
Gorman, R.M., Bryan, K.R., Laing, A.K., 2003a. Wave hindcast for the New Zealand region: deep-water wave climate. N. Z. J. Mar. Freshw. Res. 37, 589–612.
Gorman, R.M., Bryan, K.R., Laing, A.K., 2003b. Wave hindcast for the New Zealand region: nearshore validation and coastal wave climate. N. Z. J. Mar. Freshw. Res. 37, 567–588.
Grant, A.P., Walsh, K.J.E., 2001. Interdecadal variability in north-east Australian tropical cyclone formation. Atmos. Sci. Lett. 2 (1–4), 9–17.
Hall, T.M., Jewson, S., 2007. Statistical modelling of North Atlantic tropical cyclone tracks. Tellus A 59 (4), 486–498.
Hall, T.M., Jewson, S., 2008. Comparison of local and basinwide methods for risk assessment of tropical cyclone landfall. J. Appl. Meteorol. Climatol. 47 (2), 361–367.
Hannah, J., Bell, R.G., 2012. Regional sea level trends in New Zealand. J. Geophys. Res. Oceans 117, C01004.
Hawkes, P.J., Gouldby, B.R., Tawn, J.A., Owen, M.W., 2002. The joint probability of waves and water levels in coastal engineering design. J. Hydraul. Res. 40 (3), 241–251.
Hoeke, R.K., et al., 2013. Widespread inundation of Pacific islands triggered by distant-source wind-waves. Glob. Planet. Chang. 108, 128–138.
Holland, G.J., 1980. An analytical model for the wind and pressure profiles in hurricanes. Mon. Weather Rev. 108, 1212–1218.
Holthuijsen, L.H., 2007. Waves in Oceanic and Coastal Waters. Cambridge University Press, (387 pp.).
Hsu, S.A., Babin, A., 2005. Estimating the radius of maximum wind via satellite during Hurricane Lili (2002) over the Gulf of Mexico. Natl. Weather Assoc. Electron. J. 6 (3), 1–6.
IPCC, 2007. Summary for policymakers. In: Solomon, S., Qin, D., Manning, M., Chen, Z., Marquis, M., Averyt, K.B., Tignor, M., Miller, H.L. (Eds.), Climate Change: The Physical Science Basis. Contribution of Working Group I to the Fourth Assessment Report of the Intergovernmental Panel on Climate Change. Cambridge University Press, Cambridge, United Kingdom and New York, NY, USA.
Jagger, T.H., Elsner, J.B., 2012. Hurricane clusters in the vicinity of Florida. J. Appl. Meteorol. Climatol. 51 (5), 869–877.
James, M.K., Mason, L.B., 2005. Synthetic tropical cyclone database. J. Waterw. Port Coast. Ocean Eng. ASCE 131 (4), 181–192.
Knapp, K.R., Kruk, M.C., Levinson, D.H., Diamond, H.J., Neumann, C.J., 2010. The international best track archive for climate stewardship (IBTrACS) unifying tropical cyclone data. Bull. Am. Meteorol. Soc. 91 (3), 363–376.
Knutson, T.R., et al., 2010. Tropical cyclones and climate change. Nat. Geosci. 3 (3), 157–163.
Kossin, J.P., Camargo, S.J., 2009. Hurricane track variability and secular potential intensity trends. Clim. Chang. 97 (1–2), 329–337.
Kuleshov, Y., Qi, L., Fawcett, R., Jones, D., 2008. On tropical cyclone activity in the Southern Hemisphere: trends and the ENSO connection. Geophys. Res. Lett. 35 (14).
Kuleshov, Y., et al., 2010. Trends in tropical cyclones in the South Indian Ocean and the South Pacific Ocean. J. Geophys. Res.-Atmos. 115.
Leslie, L.M., Karoly, D.J., Leplastrier, M., Buckley, B.W., 2007. Variability of tropical cyclones over the Southwest Pacific Ocean using a high-resolution climate model. Meteorog. Atmos. Phys. 97 (1–4), 171–180.
Madsen, H., Jakobsen, F., 2004. Cyclone induced storm surge and flood forecasting in the northern Bay of Bengal. Coast. Eng. 51 (4), 277–296.
McInnes, K.L., et al., 2014. Quantifying storm tide risk in Fiji due to climate variability and change. Glob. Planet. Chang. 116, 115–129.
Neumann, C.J., McAdie, C.J., Amer Meteorol, S.O.C., 1997. The Atlantic tropical cyclone file: a critical need for a revision. 22nd Conference on Hurricanes and Tropical Meteorology, pp. 401–402.

Ramsay, H.A., Camargo, S.J., Kim, D., 2012. Cluster analysis of tropical cyclone tracks in the Southern Hemisphere. Clim. Dyn. 39 (3–4), 897–917.
Rayner, N.A., Parker, D.E., Horton, E.B., Folland, C.K., Alexander, L.V., Rowell, D.P., Kent, E.C., Kaplan, A., 2003. Global analyses of sea surface temperature, sea ice, and night marine air temperature since the late nineteenth century. J. Geophys. Res. 108 (D14), 4407.
Revell, C.G., Goulter, S.W., 1986. South Pacific tropical cyclones and the Southern Oscillation. Mon. Weather Rev. 114, 1138–1145.
Ross, D., 1976. A simplified model for forecasting hurricane generated waves. Bulletin of the American Meteorological Society. Presented at Conference on Atmospheric and Oceanic Waves, Seattle, Washington, March 29–April 2.
Rumpf, J., Weindl, H., Hoeppe, P., Rauch, E., Schmidt, V., 2007. Stochastic modelling of tropical cyclone tracks. Math. Meth. Oper. Res. 66 (3), 475–490.
Rumpf, J., Weindl, H., Hoeppe, P., Rauch, E., Schmidt, V., 2009. Tropical cyclone hazard assessment using model-based track simulation. Nat. Hazards 48 (3), 383–398.
Rumpf, J., Weindl, H., Faust, E., Schmidt, V., 2010. Structural variation in genesis and landfall locations of North Atlantic tropical cyclones related to SST. Tellus Ser. A Dyn. Meteorol. Oceanogr. 62 (3), 243–255.
Russell, L.R., 1971. Probability distributions for hurricane effects. J. Waterw. Harb. Coast. Eng. Div. 97, 137–154.
Salinger, M.J., et al., 1995. Climate trends in the South-west Pacific. Int. J. Climatol. 15 (3), 285–302.
Salinger, M.J., Renwick, J.A., Mullan, A.B., 2001. Interdecadal Pacific Oscillation and South Pacific climate. Int. J. Climatol. 21 (14), 1705–1721.
Santoso, A., et al., 2013. Late-twentieth-century emergence of the El Niño propagation asymmetry and future projections. Nature 504, 126–130.
Sinclair, M.R., 2002. Extratropical transition of Southwest Pacific tropical cyclones. Part I: climatology and mean structure changes. Mon. Weather Rev. 130 (3), 590–609.
Skamarock, W.C., Klemp, J.B., Dudhia, J., Gill, D.O., Barker, D.M., Duda, M., Huang, X.-Y., Wang, W., Powers, J.G., 2008. A description of the advanced research WRF version 3. NCAR Technical Note NCAR/TN-475+STR (113 pp.).
Stephens, S.A., Gorman, R.M., 2006. Extreme wave predictions around New Zealand from hindcast data. N. Z. J. Mar. Freshw. Res. 40 (3), 399–411.
Stephens, S.A., Ramsay, D., 2012. Climate Change Impacts on Coastal Inundation at Oneroa Village, Mangaia. A Geospatial Framework for Climate Change Adaptation in the Coastal Zone of Mangaia, Cook Islands. NIWA, Hamilton (HAM2012-022).
Terry, J.P., Gienko, G., 2010. Climatological aspects of South Pacific tropical cyclones, based on analysis of the RSMC-Nadi (Fiji) regional archive. Clim. Res. 42 (3), 223–233.
Tournadre, J., Ezraty, R., 1990. Local climatology of wind and sea state by means of satellite radar altimeter measurements. J. Geophys. Res. 95, 18255–18268.
Trenberth, K.E., 1997. The definition of El Niño. Bull. Am. Meteorol. Soc. 78 (12), 2771–2777.
Vickery, P.J., Twisdale, L.A., 1995. Prediction of hurricane wind speeds in the United-States. J. Struct. Eng. ASCE 121 (11), 1691–1699.
Vickery, P.J., Wadhera, D., 2008. Statistical models of Holland pressure profile parameter and radius to maximum winds of hurricanes from flight-level pressure and H*Wind data. J. Appl. Meteorol. Climatol. 47 (10), 2497–2517.
Vickery, P.J., Skerlj, P.F., Steckley, A.C., Twisdale, L.A., 2000a. Hurricane wind field model for use in hurricane simulations. J. Struct. Eng. ASCE 126 (10), 1203–1221.
Vickery, P.J., Skerlj, P.F., Twisdale, L.A., 2000b. Simulation of hurricane risk in the US using empirical track model. J. Struct. Eng. ASCE 126 (10), 1222–1237.
Vincent, D.G., 1994. The South Pacific Convergence Zone (SPCZ): a review. Mon. Weather Rev. 122 (9), 1949–1970.
Vincent, E., et al., 2011. Interannual variability of the South Pacific Convergence Zone and implications for tropical cyclone genesis. Clim. Dyn. 36 (9–10), 1881–1896.
Vinoth, J., Young, I.R., 2011. Global estimates of extreme wind speed and wave height. J. Clim. 24 (6), 1647–1665.
Walsh, K.J.E., Nguyen, K.C., McGregor, J.L., 2004. Fine-resolution regional climate model simulations of the impact of climate change on tropical cyclones near Australia. Clim. Dyn. 22 (1), 47–56.
Walsh, K.J.E., McInnes, K.L., McBride, J.L., 2012. Climate change impacts on tropical cyclones and extreme sea levels in the South Pacific — a regional assessment. Glob. Planet. Chang. 80–81, 149–164.
Wang, B., Chan, J.C.L., 2002. How strong ENSO events affect tropical storm activity over the Western North Pacific. J. Clim. 15 (13), 1643–1658.
Warner, T.T., Anthes, R.A., McNab, A.L., 1978. Numerical simulations with a three dimensional mesoscale model. Mon. Weather Rev. 106, 1079–1099.
Widlansky, M.J., Webster, P.J., Hoyos, C.D., 2011. On the location and orientation of the South Pacific Convergence Zone. Clim. Dyn. 36 (3–4), 561–578.
Yasuda, T., Mase, H., Mori, N., 2010. Projection of future typhoons landing on Japan based on a stochastic typhoon model utilizing AGCM projections. Hydrol. Res. Lett. 4, 65–69.
Yonekura, E., Hall, T.M., 2011. A statistical model of tropical cyclone tracks in the Western North Pacific with ENSO-dependent cyclogenesis. J. Appl. Meteorol. Climatol. 50 (8), 1725–1739.
Young, I.R., 1988. Parametric hurricane wave prediction model. J. Waterw. Port Coast. Ocean Eng. ASCE 114 (5), 637–652.
Young, I.R., 1994. Global ocean wave statistics obtained from satellite observations. Appl. Ocean Res. 16 (4), 235–248.
Young, I.R., 1999. Seasonal variability of the global ocean wind and wave climate. Int. J. Climatol. 19 (9), 931–950.